

The QCD equation of state at finite density from analytical continuation

J. Günther¹, R. Bellwied⁵, S. Borsanyi¹, Z. Fodor^{1,2,3}, S. D. Katz^{2,4}, A. Pasztor¹, C. Ratti⁵

¹ *Department of Physics, University of Wuppertal,
Gaussstr. 20, D-42119 Wuppertal, Germany*

² *Inst. for Theoretical Physics, Eötvös University,
Pázmány P. sétány 1/A, H-1117 Budapest, Hungary*

³ *Jülich Supercomputing Centre,
Forschungszentrum Jülich, D-52425 Jülich, Germany*

⁴ *MTA-ELTE "Lendület" Lattice Gauge Theory Research Group,
Pázmány P. sétány 1/A, H-1117 Budapest, Hungary*

⁵ *Department of Physics, University of Houston,
Houston, TX 77204, USA*

(Dated: March 2, 2022)

We determine the equation of state of QCD at finite chemical potential, to order $(\mu_B/T)^6$, for a system of 2+1 quark flavors. The simulations are performed at the physical mass for the light and strange quarks on several lattice spacings; the results are continuum extrapolated using lattices of up to $N_t = 16$ temporal resolution. The QCD pressure and interaction measure are calculated along the isentropic trajectories in the (T, μ_B) plane corresponding to the RHIC Beam Energy Scan collision energies. Their behavior is determined through analytic continuation from imaginary chemical potentials of the baryonic density. We also determine the Taylor expansion coefficients around $\mu_B = 0$ from the simulations at imaginary chemical potentials. Strangeness neutrality and charge conservation are imposed, to match the experimental conditions.

The Beam Energy Scan performed at the Relativistic Heavy Ion Collider (RHIC) constitutes a major effort to explore the phase diagram of QCD at finite density: by decreasing the collision energy, the net baryonic density of the system created in the collision can be increased. This allows to scan the phase diagram of QCD through a change in the initial temperatures and densities.

The experimental program is supplemented by a steady theoretical effort, to provide an understanding and a realistic description of the data. Lattice simulations are one of the main theoretical tools to study the QCD phase diagram. However, the sign problem limits their range of applicability to relatively small chemical potentials; the main methods which have been proposed to circumvent this problem are: multi-parameter reweighting techniques [1–4], Taylor expansion of the thermodynamic observables around $\mu_B = 0$ [5–9], analytical continuation from imaginary chemical potentials [10–17] and the density of state method: [18]. More recent approaches are represented by the use of dual variables [19], and the complex Langevin equation [20, 21]. However, their application to QCD with physical parameters and controlled discretization has not yet been achieved.

Among the most sought-after observables, the finite-density equation of state plays a fundamental role in our understanding of QCD, not only because it serves as an input for any hydrodynamic approach to the matter created in heavy ion experiments, but also because it is the main ingredient in the description of astronomic objects such as dense stars. Even if these stars involve temperature and density values which are presently not accessible by first-principle calculations, any progress on the equa-

tion of state from lattice simulations can help to build a bridge between the low-density, high temperature region of the phase diagram and the high-density, low temperature one.

The equation of state of QCD at $\mu_B = 0$ is known with good accuracy in the continuum limit [22–25], and is a standard component of state-of-the art hydrodynamic description of heavy ion collisions. Extensions to finite chemical potential are presently under control up to order $(\mu_B/T)^2$ [26]. Expansion to order $(\mu_B/T)^4$ was only attempted away from the continuum limit [27]. In this letter we calculate the $(\mu_B/T)^4$ and $(\mu_B/T)^6$ order for the first time with physical quark masses and in the continuum limit. This allows a reliable determination of the equation of state up to $\mu_B/T \simeq 2$, compatible with the RHIC energies down to $\sqrt{s} = 14.5$ GeV. The main computational challenge so far was to obtain a precise determination of the fourth and sixth order Taylor expansion coefficient, c_4 and c_6 , which are notoriously very noisy [6, 27]. In fact, the recent developments in lattice techniques have lead to much smaller discretization effects in the pion sector. It turned out that in older works the very same discretization effects have reduced noise in these coefficients. The traditional technique finds the c_4 and c_6 coefficients from the non-Gaussianity of the fluctuations of conserved charges. In large simulation volumes, however, the central limit theorem reduces these below the level of detection. With physical quark masses, fine and large lattices one must seek for an alternative technique.

Here we will show that the analytical continuation of the baryonic density from imaginary chemical potential allows to obtain c_6 in the continuum limit.

We also determine the isentropic trajectories in the (T, μ_B) plane, which the system created in a heavy-ion collision follows if dissipations are negligible. These trajectories are determined by imposing that the entropy per particle number S/N_B is conserved during the evolution, and matches the ones determined at the freeze-out for each collision energy. The calculation of the ratio S/N_B at the freeze-out values for T and μ_B , and of the isentropic trajectories corresponding to the value at the freeze-out, are performed for the first time to order $(\mu_B/T)^6$. Selected thermodynamic quantities (pressure and interaction measure) are calculated along these trajectories.

The equation of state at finite density can be written as a Taylor expansion around $\mu_B/T = 0$:

$$\frac{p(\mu_B)}{T^4} = c_0(T) + c_2(T) \left(\frac{\mu_B}{T}\right)^2 + c_4(T) \left(\frac{\mu_B}{T}\right)^4 + c_6(T) \left(\frac{\mu_B}{T}\right)^6 + \mathcal{O}(\mu_B^8). \quad (1)$$

The Taylor coefficients c_0 , c_2 , c_4 , c_6 can be calculated on the lattice. The continuum extrapolated result for c_2 was presented for the first time in [26]; c_4 was calculated at the physical point [27] but only at finite lattice spacing. Here we will present continuum extrapolated results, at the physical mass, for all of them. Our results are obtained by imposing the following conditions:

$$\langle n_S \rangle = 0 \quad \text{and} \quad \langle n_Q \rangle = 0.4 \langle n_B \rangle. \quad (2)$$

The method through which we determine $\mu_S(\mu_B)$ and $\mu_Q(\mu_B)$ to satisfy these requirements was introduced in [28]: the simulations are performed at matching strange chemical potentials, such that $n_S = 0$ and $n_Q = 0.5n_B$. From the simulation we first calculate the imaginary densities n_B, n_Q and n_S and use higher derivatives in μ_S and μ_Q to extrapolate all used observables to the desired condition (2). The Taylor coefficients in Eq. (1) are the directional derivatives along the line in the (μ_B, μ_S, μ_Q) space, set by the condition in Eq. (2), calculated at $\mu_B = 0$.

We simulate at six values of imaginary chemical potentials $\mu_B^{(j)} = iT\pi j/8$, $j = 3, 4, 5, 6, 6.5$ and 7. The principal quantity that we determine in each simulation point at zero and imaginary μ_B is:

$$\frac{n}{\mu_B T^2} = \frac{T}{\mu_B} \frac{d(p/T^4)}{d(\mu_B/T)} \Big|_{\langle n_S \rangle=0, \langle n_Q \rangle=0.4 \langle n_B \rangle, T=\text{const}} \quad (3)$$

Note that n is related to the baryon number density as $\frac{n}{n_B} = 1 + 0.4 \frac{d\mu_Q}{d\mu_B}$. The first few terms in its Taylor expansion are: $2c_2 + 4c_4(\mu_B/T)^2 + 6c_6(\mu_B/T)^4$: taking derivatives of $n/(\mu_B T^2)$ with respect to μ_B , we can therefore obtain the desired Taylor coefficients. It turns out that this method allows a more precise determination of these quantities, compared to the direct simulation at $\mu_B = 0$.

These data are augmented by a $j = 0$ data set for all lattices that we used to calculate the Taylor coefficients

using the standard technique. We used the c_2 data from the $j = 0$ runs to calculate the $\mu_B \rightarrow 0$ limit of $n/(\mu_B T^2)$, which we analyzed along with the other simulations with imaginary μ_B . These $\mu_B = 0$ simulations and the here used methods for the generalized quark number susceptibilities have already been described in Ref. [29].

Our continuum extrapolation is based on the following lattices: $40^3 \times 10$, $48^3 \times 12$ and $64^3 \times 16$, in the 4stout staggered discretization. We refer to the corresponding data sets by the Euclidean temporal resolution $N_t=10$, 12 and 16, respectively. (The $j = 6.5$ data set consists of $N_t = 10$ and $N_t = 12$.) For the details of the lattice action and ensemble parameters see Ref. [29]. We note that the action in use has a dynamical charm degree of freedom, i.e. we actually simulate 2+1+1 flavor ensembles for this paper. In Eq. (3), however, the charm contribution is deliberately not added (it would be negligible in our temperature range, anyway), and the charm quark does not couple to the μ_B chemical potential in our implementation. We take c_0 from the already published $\mu_B = 0$ equation of state with 2+1 dynamical flavors [23]. Thus, the results that we present here refer to the 2+1 flavor theory. We have shown in our recent work that the effect of the charm quark is very small for the temperatures of interest in this paper [25].

For each of the above chemical potentials ($\mu_B \neq 0$) we run our simulations at 16 temperature values between 135 and 220 MeV. For higher temperatures, $T > T_{\text{connect}}$, we restrict our study to c_2 and c_4 based on the data at $\mu_B = 0$. This is justified because, as we will see, c_6 is consistent with zero for $T \geq 200$ MeV. We consider two values for this temperature cut: $T_{\text{connect}} = 200$ MeV and $T_{\text{connect}} = 220$ MeV.

The runs on the different lattices do not correspond to the exact same values of the temperature. Therefore we interpolate each set of $n/(\mu_B T^2)$ data with fixed imaginary μ_B/T and lattice resolution separately in temperature using the following four functions:

$$\begin{aligned} A_1(T) &= a + bT + c/T + d \arctan(e(T-f)) \\ A_2(T) &= a + bT + c/T + d/(1 + e(T-f)^g)^{1/g}, \\ A_3(T) &= a + bT + cT^2 + d \arctan(e(T-f)) \\ A_4(T) &= a + bT + cT^2 + d/(1 + e(T-f)^g)^{1/g}. \end{aligned} \quad (4)$$

The functions $A_{1...4}$ are strictly meant as interpolation, the range of validity obviously cannot extend to very high or very low temperatures. For $T > T_{\text{connect}}$ we use the $\mu_B = 0$ simulations to extrapolate $n/\mu_B T^2$ to each simulated imaginary μ_B/T parameter. This way we can use the functions (4) in the full temperature range.

The interpolation is necessary to align the data points to the same temperature for a given scale setting definition, and to enable us to take the derivative with respect to the temperature itself, which is needed for the entropy and energy density. This introduces a correlation between the data at different temperatures: for this

reason, from this point on we analyze the different temperatures separately. We consider two different scale settings, by fixing f_π and w_0 to their physical values. The scale setting procedure, and details on the $\mu = 0$, $T > 0$ ensembles are given in Ref. [29].

We fit the μ_B^2 -dependence of $n(\mu_B, T)/\mu_B T^2$ with three functions:

$$\begin{aligned} B_1(\hat{\mu}) &= a + b\hat{\mu}^2 + c\hat{\mu}^4 \\ B_2(\hat{\mu}) &= (a + b\hat{\mu}^2)/(1 + c\hat{\mu}^2) \\ B_3(\hat{\mu}) &= a + b\hat{\mu}^2 + c \sin(\hat{\mu})/\hat{\mu} \end{aligned} \quad (5)$$

where $\hat{\mu} = i\mu_B/T$ is a real parameter in our simulations. The first two functions, polynomial and Padé, are taken as two natural choices when no prior information on the physics is available. They are two extremes in the sense, that c_8/c_6 is zero in B_1 , but large in B_2 . The third function reflects our physical expectations at very low and very high temperatures: below the transition the Hadron Resonance Gas picture predicts that the μ_B -dependent part of the free energy is proportional to $\cosh(\mu_B/T)$, which translates to $\sin(\hat{\mu})$ for the imaginary density. On the other hand, at infinite temperature the a and b coefficients exactly describe the physics.

The extrapolation to real μ_B is performed from the above functional forms: an example is shown in Fig. 1, where we show the analytical continuation of $n/(\mu_B T^2)$ from negative to positive $(\mu_B/T)^2$ for two different temperatures, and $N_t = 12$. This plot illustrates the challenge of analytical continuation: several functions describe the data on the $\mu_B^2 < 0$ side equally well, but they differ for $\mu_B^2 > 0$. The systematic error, that we estimate (among other effects) by varying the fit function, is similar in size to the statistical uncertainty (calculated using the bootstrap method).

We introduce two options for the continuum extrapolation: In the first round we fit the results corresponding to the three N_t separately and extract the a , b , c coefficients for each one of them. We then obtain their continuum limit from a linear fit in $1/N_t^2$. The second option is to combine the fitting of the μ_B -dependence with the continuum extrapolation. Consider e.g. the B_1 function above. We write it as:

$$\begin{aligned} B_1(\hat{\mu}; N_t) &= a_1 + a_2/N_t^2 + b_1\hat{\mu}^2 + b_2\hat{\mu}^2/N_t^2 \\ &\quad + c_1\hat{\mu}^4 + c_2\hat{\mu}^4/N_t^2. \end{aligned} \quad (6)$$

In this way we obtain the continuum limit and the μ_B -dependence fit simultaneously.

In total we have 96 different analyses, each one of which produces acceptable fits; the width of their distribution (with uniform weights) is used as systematic error. For each shown quantity we give the combined error, namely the statistical and systematic errors added in quadrature.

In Figure 2 we show the temperature dependence of the Taylor expansion coefficients c_0, \dots, c_6 in the continuum limit for the pressure. Here c_0 is taken from our

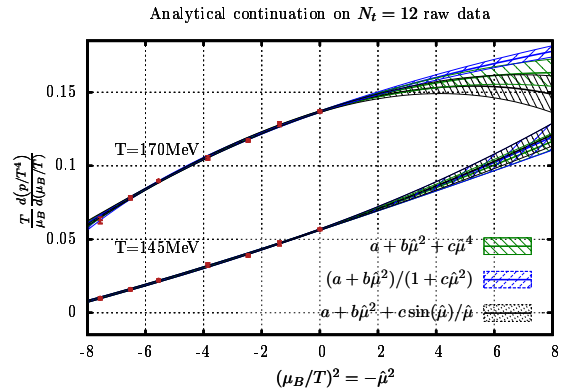


FIG. 1. Analytical continuation of $n/(\mu_B T^2)$ from negative to positive $(\mu_B/T)^2$ for $T = 145$ MeV (lower curves) and $T = 170$ MeV (upper curves) and $N_t = 12$. The different colors correspond to different fitting functions from Eqs. (5). The curves intersect $\mu_B = 0$ at $2c_2(T)$, the slope and curvature at $\mu_B = 0$ give c_4 and c_6 , respectively. The plots suggests, that c_6 is negative above T_c , and, with marginal statistical significance, it is positive below T_c .

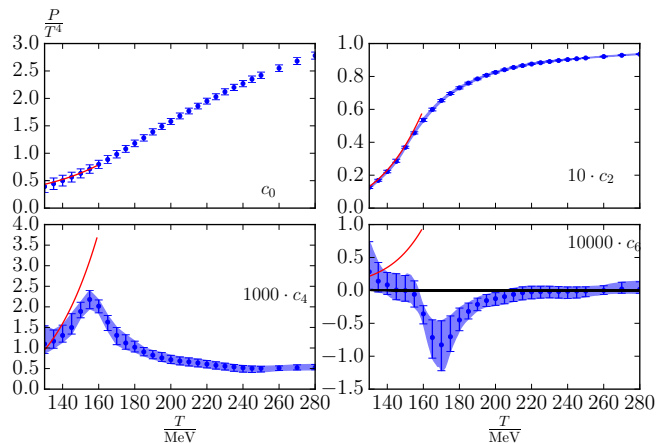


FIG. 2. Coefficients c_0, \dots, c_6 for the Taylor expansion of the pressure around $\mu_B = 0$. The data are continuum extrapolated and they are presented as functions of the temperature along with the HRG prediction (red lines).

earlier $\mu = 0$ work [23]. Notice that c_6 presents a dip at a temperature slightly larger than the QCD transition temperature, as predicted by chiral models [30]. Besides, c_6 is compatible with zero at $T \geq 200$, which makes the use of the Taylor expansion above this temperature justified. The non-vanishing error on c_6 above 220 MeV shows the intrinsic systematic error of our approach, that includes the use of the temperature fit Eq. (4) and the μ_B/T functions $B_{1...3}$ in the entire temperature range.

The other quantities are related to the pressure by thermodynamic identities. The energy density is defined as $\varepsilon = Ts - p + \sum_i \mu_i n_i$, where $s = [T^4 \partial/\partial T + 4T^3](p/T^4)$ is the entropy density and $i = B, Q$. The $i = S$ term could be dropped because of the strangeness neutrality

condition. We used the corresponding μ_B, μ_Q, n_B and n_Q values at each given simulation point. For the T -derivative in the entropy density we used the derivatives of the already fitted functions (4). The naive T derivative of these fit functions is a directional derivative along constant μ_B/T and variable μ_Q and μ_S defined by Eq. (2). Using the temperature dependence of μ_Q one can calculate the partial T -derivative that defines the entropy. The terms in ε and s that are related to the variable μ_Q/T in a fixed- μ_B/T dataset are smaller than the overall error. Nevertheless, in the numerical analysis none of the terms were dropped.

Therefore it is possible to obtain all the thermodynamic quantities at finite chemical potential. In particular, we start with the entropy density s and baryonic density n_B . These quantities are relevant because, in the absence of dissipative effects, the medium created in a heavy ion collision expands without generation of entropy (S) and with a fixed baryon number (N_B), so that $S/N_B = s/n_B$ is fixed in this case. We calculate the ratio s/n_B for the values of the freeze-out temperatures and chemical potentials extracted in Ref. [31], which correspond to the various collision energies of the RHIC beam energy scan. After the initial collision, the system starts from a point in the (T, μ_B) plane and follows a trajectory which will bring it to one of the freeze-out points. We start from the freeze-out points and reconstruct the isentropic trajectories backwards in the (T, μ_B) plane. This is done for the first time from lattice QCD simulations to order μ_B^6 . Such isentropic trajectories are shown in Fig. 3. The black points are the freeze-out parameters from Ref. [31]. The last point corresponds to the preliminary analysis of the new STAR run at 14.5 GeV [32]. The curves are continued in the hadronic phase by means of the Hadron Resonance Gas (HRG) model.

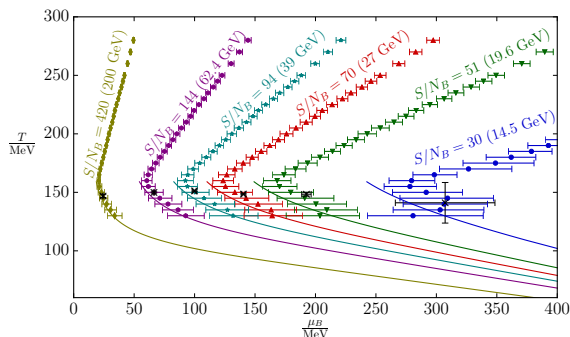


FIG. 3. The QCD phase diagram in the (T, μ_B) plane with the isentropic trajectories: the contours with fixed S/N_B value. The green points are the chemical freeze-out parameters extracted in Ref. [31]. The S/N_B ratios correspond to the RHIC energies 200, 62.4, 39, 27, 19.6 and 14.5 GeV. The last point is based on preliminary STAR data [32]. The freeze-out parameters are obtained by a combined fit of net-electric charge and net-proton fluctuations in the HRG model.

We use the continuum extrapolated fit parameters and the formulas in Eq. (5) to extrapolate the pressure and the trace anomaly to finite density. In Fig. 4 we plot these observables for two of the RHIC energies along the isentropic trajectories of Fig. 3. The effect of the finite chemical potential is more prominent at high temperature for the pressure, while the interaction measure is mildly affected by the change in μ_B , and mainly at low temperatures.

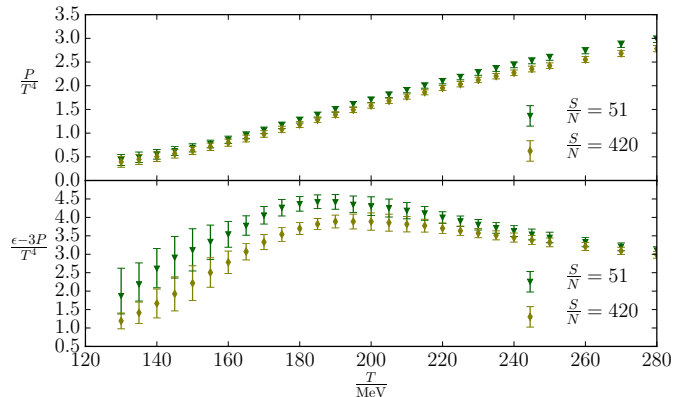


FIG. 4. Pressure (upper panel) and interaction measure (lower panel) as functions of temperature, calculated along the highest and lowest isentropic trajectories from Fig. 3.

In conclusion, we have presented lattice QCD results for the Taylor expansion coefficients of the pressure up to order $(\mu_B/T)^6$. These results, simulated at the physical mass and continuum extrapolated, are achieved for the first time in this paper, using to the method of analytical continuation of the baryonic density from imaginary chemical potential and taking its derivatives with respect to μ_B . As our results indicate, this approach leads to a more precise determination of the coefficients, as compared to their direct simulation at $\mu_B = 0$. Starting from the freeze-out parameters of Ref. [31], we have then determined the isentropic trajectories in the (T, μ_B) plane up to order $(\mu_B/T)^6$, and calculated the pressure and interaction measure along these trajectories. The results presented here allow to reliably extend the calculations of the thermodynamic quantities up to $\mu_B/T \simeq 2$, which covers most of the Beam Energy Scan program at RHIC.

ACKNOWLEDGEMENTS

C.R. would like to thank Volker Koch, Jacquelyn Noronha-Hostler, Jorge Noronha and Bjorn Schenke for fruitful discussions. This project was funded by the DFG grant SFB/TR55. This material is based upon work supported by the National Science Foundation through grant number NSF PHY-1513864 and by the U.S. Department of Energy, Office of Science, Office of Nuclear Physics,

within the framework of the Beam Energy Scan Theory (BEST) Topical Collaboration. An award of computer time was provided by the INCITE program. This research used resources of the Argonne Leadership Computing Facility, which is a DOE Office of Science User Facility supported under Contract DE-AC02-06CH11357. The authors gratefully acknowledge the Gauss Centre for Supercomputing (GCS) for providing computing time for a GCS Large-Scale Project on the GCS share of the supercomputer JUQUEEN [33] at Jülich Supercomputing Centre (JSC).

-
- [1] Z. Fodor and S. D. Katz, Phys. Lett. **B534**, 87 (2002), arXiv:hep-lat/0104001 [hep-lat].
 - [2] Z. Fodor and S. D. Katz, JHEP **03**, 014 (2002), arXiv:hep-lat/0106002 [hep-lat].
 - [3] F. Csikor, G. I. Egri, Z. Fodor, S. D. Katz, K. K. Szabo, and A. I. Toth, JHEP **05**, 046 (2004), arXiv:hep-lat/0401016 [hep-lat].
 - [4] Z. Fodor and S. D. Katz, JHEP **04**, 050 (2004), arXiv:hep-lat/0402006 [hep-lat].
 - [5] C. R. Allton, S. Ejiri, S. J. Hands, O. Kaczmarek, F. Karsch, E. Laermann, C. Schmidt, and L. Scorzato, Phys. Rev. **D66**, 074507 (2002), arXiv:hep-lat/0204010 [hep-lat].
 - [6] C. R. Allton, M. Doring, S. Ejiri, S. J. Hands, O. Kaczmarek, F. Karsch, E. Laermann, and K. Redlich, Phys. Rev. **D71**, 054508 (2005), arXiv:hep-lat/0501030 [hep-lat].
 - [7] R. V. Gavai and S. Gupta, Phys. Rev. **D78**, 114503 (2008), arXiv:0806.2233 [hep-lat].
 - [8] S. Basak *et al.* (MILC), *Proceedings, 26th International Symposium on Lattice field theory (Lattice 2008)*, PoS **LATTICE2008**, 171 (2008), arXiv:0910.0276 [hep-lat].
 - [9] O. Kaczmarek, F. Karsch, E. Laermann, C. Miao, S. Mukherjee, P. Petreczky, C. Schmidt, W. Soeldner, and W. Unger, Phys. Rev. **D83**, 014504 (2011), arXiv:1011.3130 [hep-lat].
 - [10] P. de Forcrand and O. Philipsen, Nucl. Phys. **B642**, 290 (2002), arXiv:hep-lat/0205016 [hep-lat].
 - [11] M. D’Elia and M.-P. Lombardo, Phys. Rev. **D67**, 014505 (2003), arXiv:hep-lat/0209146 [hep-lat].
 - [12] L.-K. Wu, X.-Q. Luo, and H.-S. Chen, Phys. Rev. **D76**, 034505 (2007), arXiv:hep-lat/0611035 [hep-lat].
 - [13] M. D’Elia, F. Di Renzo, and M. P. Lombardo, Phys. Rev. **D76**, 114509 (2007), arXiv:0705.3814 [hep-lat].
 - [14] S. Conradi and M. D’Elia, Phys. Rev. **D76**, 074501 (2007), arXiv:0707.1987 [hep-lat].
 - [15] P. de Forcrand and O. Philipsen, JHEP **11**, 012 (2008), arXiv:0808.1096 [hep-lat].
 - [16] M. D’Elia and F. Sanfilippo, Phys. Rev. **D80**, 014502 (2009), arXiv:0904.1400 [hep-lat].
 - [17] J. T. Moscicki, M. Wos, M. Lamanna, P. de Forcrand, and O. Philipsen, Comput. Phys. Commun. **181**, 1715 (2010), arXiv:0911.5682 [cs.DC].
 - [18] Z. Fodor, S. D. Katz, and C. Schmidt, JHEP **0703**, 121 (2007), arXiv:hep-lat/0701022 [hep-lat].
 - [19] C. Gattlinger, *Proceedings, 31st International Symposium on Lattice Field Theory (Lattice 2013)*, PoS **LATTICE2013**, 002 (2014), arXiv:1401.7788 [hep-lat].
 - [20] E. Seiler, D. Sexty, and I.-O. Stamatescu, Phys. Lett. **B723**, 213 (2013), arXiv:1211.3709 [hep-lat].
 - [21] D. Sexty, Phys. Lett. **B729**, 108 (2014), arXiv:1307.7748 [hep-lat].
 - [22] S. Borsanyi, G. Endrodi, Z. Fodor, A. Jakovac, S. D. Katz, S. Krieg, C. Ratti, and K. K. Szabo, JHEP **11**, 077 (2010), arXiv:1007.2580 [hep-lat].
 - [23] S. Borsanyi, Z. Fodor, C. Hoelbling, S. D. Katz, S. Krieg, and K. K. Szabo, Phys. Lett. **B730**, 99 (2014), arXiv:1309.5258 [hep-lat].
 - [24] A. Bazavov *et al.* (HotQCD), Phys. Rev. **D90**, 094503 (2014), arXiv:1407.6387 [hep-lat].
 - [25] S. Borsanyi *et al.*, (2016), arXiv:1606.07494 [hep-lat].
 - [26] S. Borsanyi, G. Endrodi, Z. Fodor, S. D. Katz, S. Krieg, C. Ratti, and K. K. Szabo, JHEP **08**, 053 (2012), arXiv:1204.6710 [hep-lat].
 - [27] P. Hegde (BNL–Bielefeld–CCNU), Nucl. Phys. **A931**, 851 (2014), arXiv:1408.6305 [hep-lat].
 - [28] R. Bellwied, S. Borsanyi, Z. Fodor, J. Günther, S. D. Katz, C. Ratti, and K. K. Szabo, Phys. Lett. **B751**, 559 (2015), arXiv:1507.07510 [hep-lat].
 - [29] R. Bellwied, S. Borsanyi, Z. Fodor, S. D. Katz, A. Pasztor, C. Ratti, and K. K. Szabo, Phys. Rev. **D92**, 114505 (2015), arXiv:1507.04627 [hep-lat].
 - [30] B. Friman, F. Karsch, K. Redlich, and V. Skokov, Eur. Phys. J. **C71**, 1694 (2011), arXiv:1103.3511 [hep-ph].
 - [31] P. Alba, W. Alberico, R. Bellwied, M. Bluhm, V. Mantovani Sarti, M. Nahrgang, and C. Ratti, Phys. Lett. **B738**, 305 (2014), arXiv:1403.4903 [hep-ph].
 - [32] X. Luo (2015) arXiv:1512.09215 [nucl-ex].
 - [33] *JUQUEEN: IBM Blue Gene/Q Supercomputer System at the Jülich Supercomputing Centre*, Tech. Rep. 1 A1 (Jülich Supercomputing Centre, <http://dx.doi.org/10.17815/jlsrf-1-18>, 2015).